Solar-Terrestrial Physics. 2024. Vol. 10. Iss. 3. P. 37–49. DOI: 10.12737/stp-103202405. © 2024 M.B. Krainev, M.S. Kalinin. Published by INFRA-M Academic Publishing House

UDC 524.1
DOI: 10.12737/stp-103202405

Received March 03, 2024
Accepted May 31, 2024

FIFTY YEARS OF STUDYING THE GCR INTENSITY DURING INVERSION OF THE HELIOSPHERIC MAGNETIC FIELDS. II. HMF INVERSION ON THE INNER HELIOSPHERIC BOUNDARY

M.B. Krainev
Lebedev Physical Institute RAS, Moscow, Russia, mkrainev46@mail.ru

M.S. Kalinin
Lebedev Physical Institute RAS, Moscow, Russia, kalininms@lebedev.ru

Abstract. Phenomena in the outer layer of the solar atmosphere, the heliosphere, including the supersonic solar wind, the heliospheric magnetic field (HMF) carried by it, and cosmic rays propagating in the heliosphere are important for many processes occurring in this layer. For some of these processes such as geomagnetic activity or propagation of cosmic rays, not only the strength, but also the direction of the field is significant. Nonetheless, if in this regard the situation during periods of low sunspot activity is quite clear — the heliosphere is divided into two hemispheres with opposite polarity (toward the Sun/away from the Sun), — during periods of high sunspot activity when the HMF inversion occurs, there is no simple model of this phenomenon.

The paper is a sequel to the study of the HMF inversion phenomenon and associated effects in the intensity of galactic cosmic rays (GCR). Previously, general ideas about the 22-year cyclicity in the characteristics of the Sun, heliosphere, and cosmic rays have been formulated, and the effects observed in the GCR intensity, which we associate with the HMF inversion, have been discussed in detail. This paper deals with a model of HMF inversion, associated only with the evolution of the magnetic field in the layer between the photosphere and the base of the heliosphere due to changes in the distribution of photospheric fields from one solar rotation to the next one, and shows that this is not enough to explain the main effects in the GCR intensity. In this layer, the magnetic field is the main energy factor. A more complete model of HMF inversion, including the transformation of its characteristics due to the interaction of different-speed solar wind streams in the heliosphere itself, where the solar wind is the main energy factor, will be discussed in the next paper.

Keywords: heliosphere, heliospheric magnetic fields (HMF), inversion of HMF, galactic cosmic rays (GCR), GCR modulation, long-term GCR variations, GCR during HMF inversion.

INTRODUCTION

The main topic of this series of papers is the description and simulation of long-term variations in the intensity of galactic cosmic rays (GCRs) caused by inversion of the heliospheric magnetic field (HMF). By long-term variations are meant variations in intensity averaged over a solar rotation, i.e., for example, Forbush decreases in intensity do not relate to long-term ones, but contribute to them. In the first part of our work [Krainev et al., 2023b], we have formulated general facts and ideas about 22-year variations in solar and heliospheric magnetic fields, and GCR intensity, and have thoroughly discussed the observed GCR intensity effects we attribute to HMF inversion. In this paper, we formulate qualitative concepts, discuss approaches, and take a step toward the development of a quantitative model of the heliosphere during HMF inversion.

Since this model is designed to simulate long-term GCR intensity variations, it should have certain features. Firstly, as GCR energy and rigidity is much higher than the energy and rigidity of thermal and even directional motion of solar wind (SW) plasma particles, the model may not include details related to these motions. Thus in this model, the structure of the heliospheric current sheet (HCS) or a set of local small-scale current sheets can be neglected. Secondly, to describe the GCR behavior even at one point deep in the heliosphere (say, at Earth's orbit), a model of the entire heliosphere is required ($0.1<r<\sim120$ AU, $0°<\theta<180°$, $0°<\varphi<360°$). The fact is that on the way to Earth, GCR particles pass through the entire heliosphere, and their path strongly depends not only on their kinetic characteristics (velocity, rigidity), but also on the sign of their electric charge. Thirdly, the higher energy of GCR particles than that of SW plasma leads to the fact that GCRs cross the heliosphere and adjust to its structure much faster ($\tau_{GCR}\leq1$ month) than this structure is formed ($\tau_{HS}\geq1$ year). To describe GCR characteristics at a given instant of time, it is therefore necessary to take into account the Sun's characteristics — first of all, the solar magnetic fields (SMFs) approximately for the previous year. Note that such a model of the heliosphere is quasi-stationary, i.e. it does not directly include transient phenomena such as coronal mass ejections etc., which we assume to disturb such a heliosphere only briefly.

At present, when simulating long-term GCR intensity variations, distortion of the characteristics observed on the Sun or in the inner heliosphere is usually neglected. It is believed, for example, that the three main observable parameters that determine the long-term modulation of GCR intensity are the degree of HCS waviness (or quasi-tilt α_{qt}) and the overall HMF polarity A, determined from data on SMF in the corona, as well as the absolute radial component of HMF from observations at

Earth's orbit (e.g., [Potgieter, 2013; Krainev et al., 2021]). Thus, it is assumed that the regularities in the distribution of polarity and HMF observed on the Sun and deep in the heliosphere do not change up to its boundary. The model of the heliosphere, we deal with in this paper, is analogous, i.e. it also takes into account magnetic field inversion, as it occurs at the inner heliospheric boundary, and extends the conditions at the inner boundary to the entire heliosphere regardless of active processes in it.

Section 1 discusses general issues of HMF formation. Qualitative concepts of the HMF inversion in past four solar cycles (SC) 21–24 according to the Zurich classification, for which photospheric SMFs were scanned and simulated in the solar corona, are examined in Section 2. Since HMF inversions occur during maximum sunspot activity, the time profile of this cycle is important for the GCR intensity effects that we associate with HMF inversion; and SC 24 and 25 differ from the previous ones. Section 3 separately analyzes the sunspot cycle and the HMF inversion in these solar cycles. Section 4 formulates a quantitative model of HMF inversion in view of magnetic field polarity reversal only in the solar corona. Section 5 employs this model to calculate the GCR intensity during HMF inversion in SC 24, and uses the results of calculations to verify the major pattern of proton and electron behavior, established for this period from the PAMELA and AMS-02 experiments. Finally, Section 6 discusses the results and draws conclusions.

1. GENERAL IDEAS ABOUT FORMATION OF THE HELIOSPHERIC MAGNETIC FIELD

According to existing ideas, HMF is formed sequentially in several layers of the Sun and its atmosphere.

1. In the layer under the photosphere, the interaction between motions of solar plasma and magnetic fields (in general, presumably described by the dynamo theory [Charbonneau, 2010]) creates two SMF branches (toroidal and poloidal) on the photosphere ($r=r_S$) with different characteristics.

2. In the layer above the photosphere ($r_S<r\le r_{SS}\approx 2.5\, r_S$) due to the rapid decrease in atmospheric density, the main energy is contained in SMF and their distribution is usually estimated in a modification of the potential magnetic field model (PMFM) [Schatten et al., 1969; Altschuler, Newkirk, 1969], in which the larger-scale poloidal branch of SMF gains an advantage. In this model, only the radial SMF component remains on the outer surface of this layer (the source surface $r=r_{SS}$) B_r^{SS} with large unipolar regions of open field lines (i.e., field lines that do not close to the photosphere, but open to the heliosphere). Neutral lines ($B_r^{SS}=0$) on this surface are considered as bases of the current sheet (although, of course, at $r<r_{SS}$ there is no current, even a current sheet). In the same (let us call it potential) layer, SW is generally accelerated along open field lines to supersonic (but not super-Alfvén) velocities.

3. In the next layer ($r_{SS}<r\le r_{in}^{HS}\approx 21.5 r_S=0.1$ AU), the SW kinetic energy density becomes comparable, and then exceeds the magnetic energy density. In this case, it is usually assumed that the distribution by SMF polarity in this layer changes slightly and in strength changes due to current sheets based on neutral lines $B_r^{SS}=0$ [Schatten, 1971].

4. Finally, in the heliosphere, where the SW kinetic energy prevails, SW and HMF characteristics are determined by their boundary conditions (as well as by boundary conditions for the SW density and temperature) in $r=r_{in}^{HS}$ and are formed by the interaction between all components, which are often considered in kinematic (i.e., neglecting the HMF effect on SW) or, more strictly, in magnetohydrodynamic (MHD) approximations.

Since the reliability of predicting the SW and HMF effects on Earth and its surrounding space depends on this, many works have delved into the processes occurring in the first three layers, from completely physical [Tóth et al., 2012] to hybrid empirical-physical [Odstrcil, 2003]. Processes in the middle and far heliosphere are not so important for assessing space weather near Earth, especially for quasi-stationary processes, primarily because at such short distances from the Sun even in a kinematic approximation we can obtain a pattern close to reality. However, in the last decade, works have appeared which are focused on constructing an SW and HMF model in all four layers of the solar atmosphere to understand, among other processes, variations in the intensity of GCRs that pass throughout the heliosphere on their way to a detector [Guo, Florinski, 2014, 2016; Wiengarten et al., 2014; Luo et al., 2020].

2. QUALITATIVE CONCEPTS OF HMF INVERSION

As already mentioned, by the mid-1970s a concept was formulated [Rosenberg, Coleman, 1969; Shulz, 1973] that during low solar activity when the heliosphere is relatively rarely disturbed by transient phenomena (such as shock waves from flares or coronal mass ejections) HMF in the first approximation proves to consist of two unipolar "hemispheres" of opposite polarity, separated by a waved HCS, and features overall polarity A (a unit quantity with the sign of radial component of regular HMF B_r in the northern hemisphere) and the degree of HCS waviness α_{qt} (the so-called quasi-tilt equal to half of the heliolatitude range occupied by HCS). The shape of HCS is usually determined from the shape of neutral lines on the source surface, calculated from WSO PMFM (Wilcox Solar Observatory, Stanford, USA, [http://wso.stanford.edu]), assuming its transfer to the heliosphere by radial SW with due regard to the rotation of the inner boundary of the heliosphere together with the Sun. The HMF strength is estimated by measured $|B_r|$ in Earth's orbit, commonly assuming that this characteristic does not depend on the heliolatitude [Smith, 2011] and the regular HMF corresponds to the Parker model [Parker, 1958].

What happens during HMF inversion at solar maxima is much worse known. It can be suspected that as a maximum is approached disturbances in the heliosphere blur the clear pattern of the two-hemisphere heliosphere with a certain overall polarity *A*. To begin with, we would like to formulate an initial model of HMF inversion caused by processes in the solar corona, i.e. under the inner heliospheric boundary. It is this model that we call the model of HMF inversion at the inner heliospheric boundary and discuss in this paper. Further, this model could be "disturbed" by a measurable parameter (for example, the number of transients per unit time) or supplemented with MHD simulation of these disturbing processes in the heliosphere.

From the results of SC simulation in different versions of the solar dynamo theory [Charbonneau, 2010] and processing the results of scanning of the photospheric magnetic field at WSO [http://wso.stanford.edu], in the GONG experiment [http://gong.nso.edu/], and at Kislovodsk Mountain Astronomical Station of the General Astronomical Observatory of the Russian Academy of Sciences (MAS GAO RAS [http://solarstation.ru/sun-service]) it is assumed that the inversion of high-latitude SMFs occurs by replacing SMF of old polarity with magnetic fields of the opposite direction due to the meridional drift or diffusion of remnants of magnetic fields of active regions from middle and low latitudes to the poles. A change and inversion of HMF polarity distribution is often described as rotation of the solar dipole relative to the axis lying approximately at the equator. This is also facilitated by the representation of the magnetic field in PMFM in the form of spherical harmonic series. In this case, a change and inversion of HMF polarity distribution should be strongly non-axisymmetric and occur in a potential layer, where the magnetic field is the main energy factor.

Our qualitative concept of HMF inversion has been formulated in [Krainev, Kalinin, 2014; Krainev et al., 2015; Krainev, 2019]. We assumed that a change and inversion of the HMF polarity distribution involve changing distribution types classified by the number and shape of neutral lines $B_r^{SS} = 0$, calculated from WSO PMFM on a source surface [http://wso.stanford.edu], and the polarity of unipolar regions on this surface. It is these lines that are considered as bases of HCS. Figure 1 illustrates the HMF polarity distribution of all five types, derived from the results of the classical version of the WSO model, by the example of HMF inversion in SC 23. Note that in PMFM the magnetic field in the layer between the photosphere and the source surface is potential, i.e. there are no currents in this layer, and the current on this surface itself is postulated only for the disappearance of the field components tangent to it.

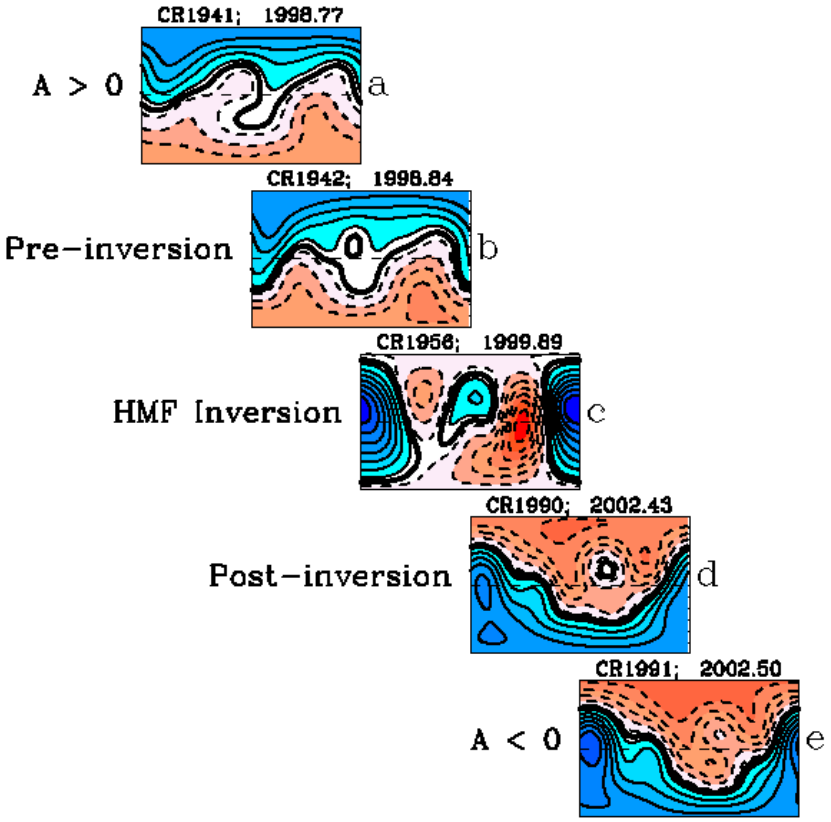

Figure 1. Phases and types of magnetic field radial component distributions on the source surface during HMF inversion in SC 23. In panels *a*–*e*, along the X-axis is the Carrington heliographic longitude $\varphi \in [0, 360]$; along the Y-axis, the latitude $\lambda \in [-90, 90]$; the number and mean time of the Carrington rotation are shown above the maps. Shades of blue and solid thin black isolines are regions of $B_r^{SS} > 0$, shades of red and dashed thin black isolines are regions of $B_r^{SS} < 0$. Bold black lines are isolines of $B_r^{SS} < 0$ (HCS bases); white, regions of small $\left|B_r^{SS}\right|$ adjacent to the line $B_r^{SS} = 0$

That is why, on the maps of Figure 1, the isolines of the field radial component indicate a smooth change in B_r^{SS} when crossing the isoline of $B_r^{SS} = 0$, and not the stepwise one characteristic of the transition through the current sheet and for observations in the heliosphere. It is, therefore, necessary to include the presence of a current sheet under (e.g., [Zhao, Hoeksema, 1994]) or above the source surface [Schatten, 1971] in the calculations for a more realistic description of the B_r distribution. When discussing the maps in Figure 1, we will pay attention only to the polarity B_r^{SS} and the shape of the neutral lines, which we will often call HCS projections.

Figure 1, *a* illustrates the distribution of HMF polarity in the last solar rotation before the beginning of the entire period of HMF inversion in SC 23. It corresponds to the overall HMF polarity $A>0$ and in Figure 2, *b*, showing the structure of the inversion periods in SC 21–24, is encoded in blue. Such a two-hemispheric (since so far we deal with only the sphere of the source surface) polarity distribution with a single and global (i.e. connecting all longitudes) HCS surface separating two unipolar hemispheres previously existed for about eight years after the end of the HMF inversion in SC 22 (Carrington rotation (CR) 1848, 1991.9, the first Carrington rotation of the dipole phase after the inversion). At the same time, the degree of HCS waviness α_{qt} systematically changed. We will call this phase of the magnetic cycle in the heliosphere, according to the type of HMF polarity distribution, dipole and color it in blue. In the pre-inversion phase (Figure 1, *b*), the HCS remains global with the same overall HMF polarity $A>0$, but during some solar rotations the HCS uniqueness is violated (in Figure 2, distribution of this type and the magnetic cycle phase are shown in blue). This is followed by the phase of the HMF inversion itself (see Figure 1, *c*) when the HCS globality is violated during some solar rotations (in Figure 2, the distribution of this type and the phase are shown in white). In the HMF post-inversion phase (see Figure 1, *d*), a global HCS is formed and maintained with a current direction corresponding to a new overall polarity $A<0$, but sometimes HCS is not unique yet (pink color in Figure 2). After completion of the entire inversion period, the HMF dipole phase again forms with two unipolar hemispheres of opposite polarity and the overall polarity $A<0$, separated by a single global HCS (GHCS) (Figure 1, *e*, red color in Figure 2), for approximately eight years (before the start of the next inversion in SC 24 (CR 2104, 2010.12, the first Carrington rotation of the pre-inversion phase)) with a change in the degree of HCS waviness.

The above behavior of HMF polarity distribution with alternating long two-hemisphere phase with single GHCS of systematically varying waviness and three HMF inversion phases of close duration at poloidal solar activity maxima has been observed since 1976 (SC 21–24). Boundaries of the HMF inversion phases during these solar cycles are tabulated in [Krainev, 2019].

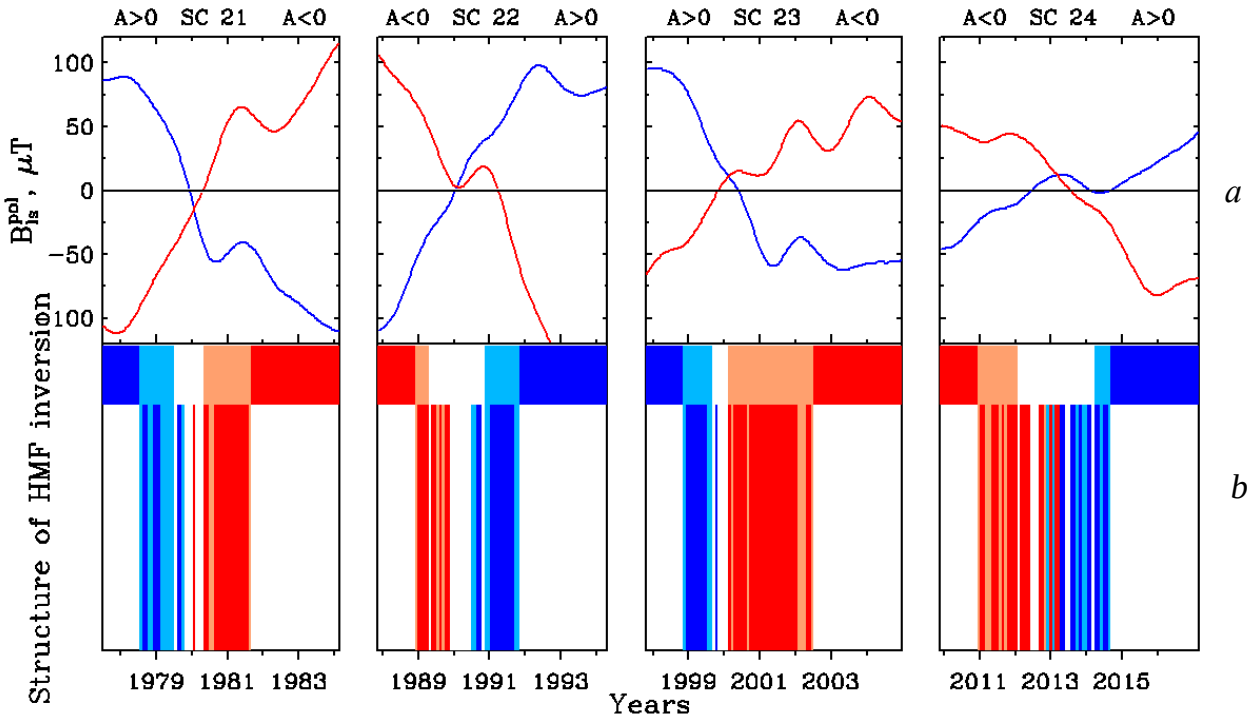

Figure 2. Inversion of high-latitude solar fields and the structure of HMF inversion periods in SC 21–24: projection smoothed with a period of one year along the line of sight of high-latitude solar fields in the northern (blue lines) and southern (red lines) polar caps [http://wso.stanford.edu/] (*a*); magnetic cycle phases in the heliosphere during HMF inversion periods (top) (*b*); sequence of HMF polarity distribution types (bottom) according to the classical version of the WSO model [Krainev, 2019]. The color coding of distribution types and magnetic cycle phases in the heliosphere is given in the text in the description of Figure 1

3. SC 24 AND 25 AS COMPARED TO OTHER CYCLES AND FEATURES OF HMF INVERSION IN SC 25

SC 24–25 are particularly interesting for two reasons. Firstly, these two cycles, weak in both the toroidal and poloidal SMF branches, differ significantly from powerful SC 17–19, 21–23 (global Modern Maximum), observed throughout the 20th century [Schove, 1983]. Secondly, for SC 24 and 25 it has become possible for the first time to study the long–term behavior of GCRs from the differential intensity of primary GCRs of different types in a wide range of energies with high accuracy (experiments PAMELA (June 2006 – January 2016) [Adriani et al., 2013, 2018] and AMS-02 (May 2011 to the present) [Aguilar et al., 2018, 2021].

Currently, the position of last and current SC in comparison with previous cycles is being widely discussed. Some researchers talk about the beginning of another global minimum such as the Maunder or Dalton minima [Stozhkov et al., 2013]; others, about their more modest place (such as the Gleisberg Minimum) [Krainev et al., 2015]. In the top panel of Figure 3, *a*, the behavior of the toroidal SMF branch over the past 100 years is compared with average cycles of these fields during the Dalton and Gleisberg minima and at the Modern Maximum (as inferred from [https://www.gaoran.ru/data base/esai]). It can be seen that SC 24 and 25 are similar in sunspot activity to SC 15 and 16 (the last two SC belong to the Gleisberg Minimum) and are significantly higher than the average cycle of the Dalton Minimum. The second feature, seen in Figure 3, *a*, is a smooth transition from the Gleisberg Minimum to the Modern Maximum, shown by the linear approximation of the maximum sunspot area for SC 16–19 (correlation coefficient ρ=0.997±0.004) and an equally smooth linear return (ρ=0.9995±0.0007) from the Modern Maximum (SC 17–23) to SC 24 (we call this cycle the beginning of the Modern Minimum). Note that, as in our other works, by the time and maximum sunspot area in each cycle we mean the average characteristics for two Gnevyshev peaks [Gnevyshev, 1967; Storini et al., 2003] over the sunspot area smoothed with a period of 13 Carrington rotations.

The bottom panel of Figure 3, *b* shows the development of the SMF poloidal branch over the past 120 years. The inversion of poloidal SMFs (and hence HMFs) is seen to occur in the period between Gnevyshev peaks (Gnevyshev Gap [Gnevyshev, 1967]; the term was introduced in [Storini et al., 2003]) or slightly earlier (for SC 23).

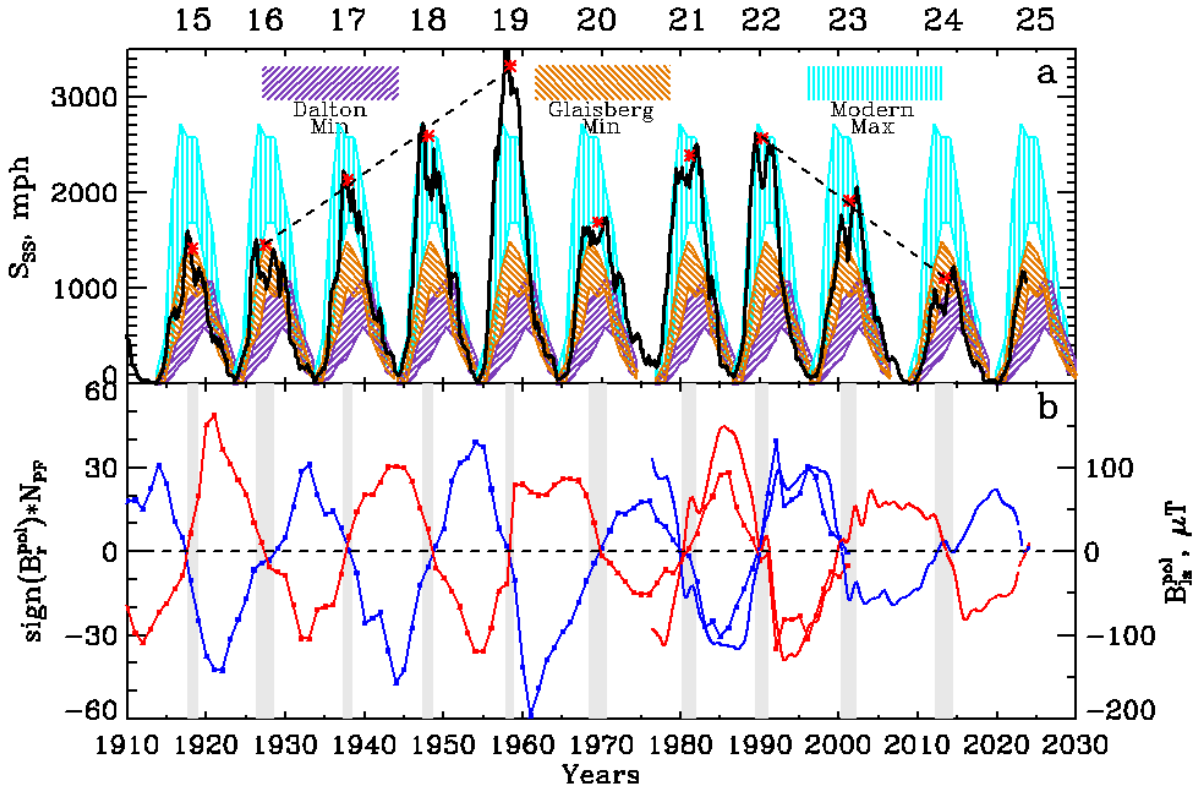

Figure 3. Toroidal and poloidal branches of solar activity from 1910 to 2024: *a* — sunspot area [https://solarscience.msfc.nasa.gov; ftp://ftp.swpc.noaa.gov/pub/forecasts/SRS], smoothed with a period of one year (black line) and the range of this characteristic superimposed on each cycle during global extremums, indicated by the corresponding color and shading (according to [https://www.gaoran.ru/database/esai]). Red icons denote the sunspot area average for two Gnevyshev peaks; dashed lines indicate a linear approximation of the transitions between periods of global extremums (see the text). Panel *b* illustrates high-latitude solar activity for the same years: for 1910–1975 — the number of polar faculae in the northern (blue line with icons) and southern (red line with icons) hemispheres [Sheeley, 1976, 2008], taken with the sign of the SMF radial component in the corresponding hemisphere; for 1976–2024 — the SMF component along the line of sight from Earth, smoothed with a 1-year period, in the northern (blue line) and southern (red line) polar caps [http://wso.stanford.edu/]

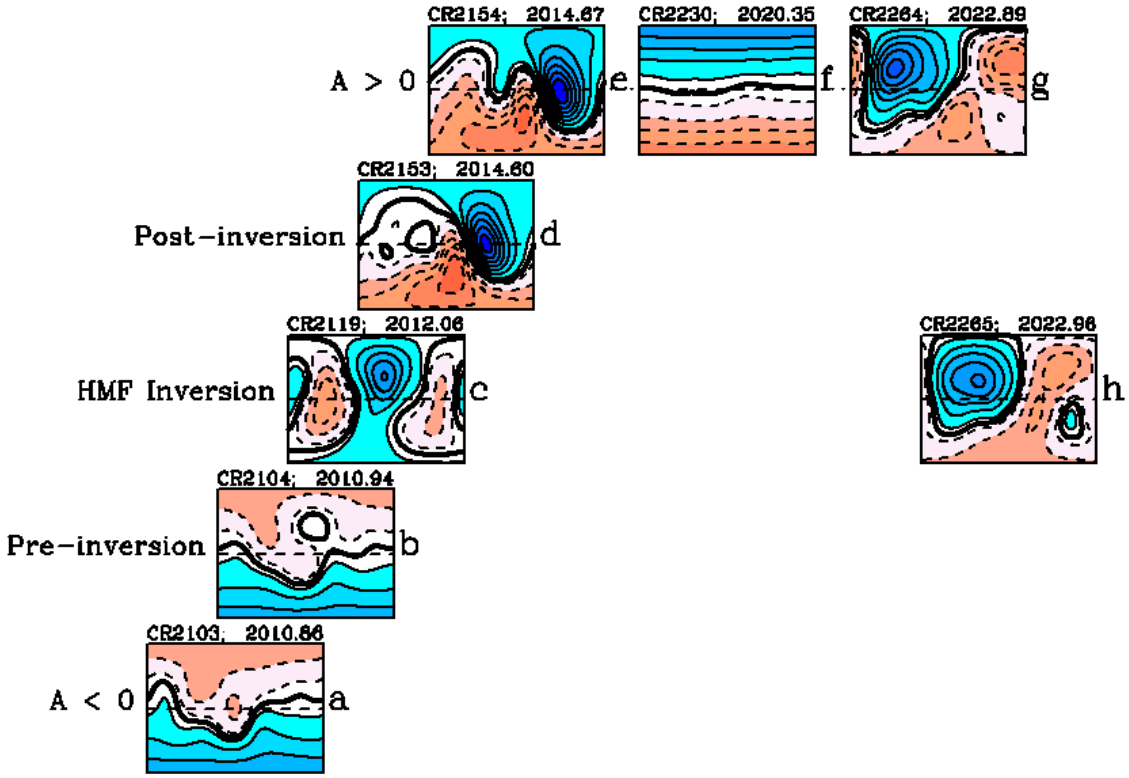

Figure 4. Main phases in HMF polarity distribution in 2010–2022 (SC 24 and 25) in accordance with the classical WSO PMFM [Krainev, 2019]. The format of all the polarity distribution maps is the same as in Figure 1

Figure 4 demonstrates the main phases of HMF inversion in SC 24 and at the beginning of SC 25 and the dipole period between the inversions. In the HMF inversion during SC 24 there are all phases we have described. A feature of the HMF inversion period in SC 25 is the absence of the pre-inversion phase: after the last rotation (CR 2264, Figure 4, *g*) of the two-hemisphere phase with single HCS and $A>0$, the phase of the HMF inversion per se with the absence of global HCS immediately began (Figure 4, *h*). In the following rotations, not shown in Figure 4, the HCS corresponding to $A<0$ appeared and disappeared, yet it is still unclear when the phase of the HMF inversion itself in SC 25 will end. This situation might be due to the fact that because of the lack of measurements in September and October 2022 the results for CR 2261–2263 are interpolated (see [http://wso.stanford.edu]). Note that the pre-inversion phase is also absent according to the results of the radial version of the WSO model, and the phase of the inversion per se began in CR 2263, two rotations earlier than in the classical version. At the same time, it is important that according to data from MAS GAO RAS [http://solarstation.ru/sun-service/forecast the HMF inversion also began in CR 2263, but with the pre-inversion phase, and the inversion itself started with CR 2267. Naturally, the pattern of the HMF inversion in SC 25 will finally be clear in a year or two.

4. QUANTITATIVE MODEL OF INTERNAL HMF INVERSION

To quantitatively describe a change and inversion of the HMF polarity distribution, it is necessary first of all to quantitatively describe the shape of the HCS surface. In a fairly general case, the regular HMF $\mathbf{B}(r, \theta, \varphi)$ in the heliosphere can be specified as

$$\mathbf{B}(r,\theta,\varphi) = \mathcal{F}(r,\theta,\varphi)\mathbf{B}^{\mathrm{m}}(r,\theta,\varphi), \tag{1}$$

where $\mathbf{B}^{\mathrm{m}}$ (r, θ, φ) is the monopole magnetic field directed everywhere from the Sun; $\mathcal{F}(r, \theta, \varphi)$ is the polarity function of regular HMF equal to +1 and –1 in respective unipolar regions [Krainev et al., 2015]. In this case, the general expression for HCS surfaces is $\mathcal{F}(r, \theta, \varphi)=0$. For the case of two-hemispheric HMF with single GHCS of a simple form

$$\mathcal{F}(r,\theta,\varphi) = A\left(1-2H\left(\theta-\theta^{\mathrm{CS}}\right)\right), \tag{2}$$

where A is the overall HMF polarity — a single value equal to +1 at $B_r>0$ in the northern unipolar hemisphere; $H(x)$ is the Heaviside function ($H(x)=1$ at $x>0$ and $H(x)=0$ at $x<0$), and θ^{CS} is the HCS polar angle at a point (r, φ).

The simplest HCS model uses the so-called tilted current sheet (TCS) models [Jokipii, Thomas, 1981]

$$\theta^{\mathrm{CS}} = \frac{\pi}{2} - \arctan\left(\tan\alpha_t \sin\left(\varphi-\omega\left(r-r_{\mathrm{in}}\right)/V_{\mathrm{sw}}\right)\right), \tag{3}$$

where ω, r_{in} and V_{sw} are the angular velocity of solar rotation, the inner size of the heliosphere, and the SW velocity respectively; α_t — the tilt or inclination of the current sheet — the angle between the plane of the solar equator and the plane in which the HCS lies at a fixed distance (the key parameter of the model). The angle α_t

is also equal to the angle between the axis of solar rotation and the axis of the magnetic dipole OZ, for which expression (3) describes the magnetic equator. Note that expressions (2) and (3) can only describe fairly simple HCS with an unambiguous function $\theta^{CS}(r, \varphi)$.

Yet, the current sheets calculated by WSO models at the base of the heliosphere (for example, Figure 1) are rather poorly described by TCS model (3), especially during medium and high sunspot activity [Krainev, Kalinin, 2010]. This is consistent with the large contribution of nondipole harmonics to the representation of the magnetic field in WSO models during these solar cycle phases. Therefore, to quantitatively describe a change and inversion of the HMF polarity distribution during high sunspot activity, we prefer to use the numerical assignment $\left\{\theta_i^{CS}, \varphi_i^{CS}\right\}$, i=1, ..., N^{CS} for each of the isolines B_r=0 (HCS bases) calculated by WSO models. Since in this paper we deal mainly with the 2D model of HMF inversion, axisymmetric with respect to the solar rotation axis, instead of the 3D function of HMF polarity $\mathcal{F}(r, \theta, \varphi)$ and the set $\left\{\theta_i^{CS}, \varphi_i^{CS}\right\}$, i=1, ..., N^{CS} for each of several HCS, we employ the longitude-averaged HMF polarity $F(r, \theta)=\langle\mathcal{F}(r, \theta, \varphi)\rangle_\varphi$ calculated taking into account all HCSs.

The sequence of different types of magnetic field polarity distribution at the base of the heliosphere described in the previous section is reflected in the stratification of this distribution in the heliosphere: the HMF polarity distribution at the base of the heliosphere, observed in a given solar rotation $T_\odot \approx 27$ days long, determines the polarity distribution in the heliospheric layer adjacent to the Sun approximately $\Delta r = T_\odot V_{sw}$ thick, where V_{sw} is the SW velocity. At the mean SW velocity ~400–500 km/s, $\Delta r \approx 7$ AU. The HMF polarity distribution in the next heliospheric layer Δr thick depends on its distribution at the base of the heliosphere in the previous solar rotation, etc. Assuming the size of the heliosphere to be ~100 AU, the magnetic field polarity distribution in the heliosphere can be represented as a set of 13–15 layers Δr, in which the type and characteristics of the HMF polarity distribution are dictated by the type and characteristics of the magnetic field polarity distribution at the base of the heliosphere in the sequence of 13–15 solar rotations. Naturally, this applies not only to the HMF polarity distribution, but also to the distribution of the modulus of its radial component, the SW velocity, etc. If such a model was to be mechanically compiled (as is done, say, in [Boschini et al., 2018]), it would not meet the basic requirements (for example, nondivergent regular HMF). Accordingly, as is often done [Potgieter, 2013; Krainev et al., 2021], to take into account the size of the heliosphere and the time of SW propagation to its boundary, we will average the characteristics observed near the Sun over this period. Next, time variations in heliospheric conditions will be determined from averages of its characteristics for the previous year or, if the characteristics averaged over solar rotation are used, from their series smoothed with a period of n_{sm}=13 and shifted by $n_{sm}/2$ rotations back in time.

Figure 5, in addition to repeating the dynamics of inversion of the high-latitude magnetic field in the solar photosphere and the structure of magnetic phases and HMF inversion periods in SC 21–24 (see Figure 2), shows how smoothed heliospheric characteristics behave. Three bottom panels exhibit time profiles of characteristics smoothed with ~1 year period: the longitude-averaged HMF polarity on the inner heliospheric boundary (more precisely, on the source surface) at the poles; the ratio of areas of regions with positive and negative magnetic field polarities also on the source surface to the longitude-averaged HMF radial component modulus in Earth's orbit. The HMF inversion at the poles at the inner heliospheric boundary is seen to occur for about one to two years in the same periods as the inversion of high-latitude photospheric magnetic fields. When calculating the longitude-averaged and smoothed HMF radial component modulus, HMF polarity is ignored. Thus, the use of this characteristic in the model suggests that areas of the regions with positive and negative HMF polarities are equal, otherwise the requirement of zero magnetic flux through the sphere is violated, which is fraught with many troubles when applying such a heliospheric model. Figure 5, *d* shows that the smoothed ratio between these areas is little different (by 10–20 %) from 1. In the behavior of the longitude-averaged HMF radial component modulus in Earth's orbit against the background of a general increase during maximum sunspot cycle, local decreases lasting 1–2 years are noticeable, which we associate with the Gnevyshev Gap [Storini et al., 2003] and the corresponding phenomena in the GCR intensity [Krainev et al., 2023a].

Figure 5, *c* depicts the time profile of HMF polarity F at the inner heliospheric boundary only at the poles. Nonetheless, as will be seen in the next section, this characteristic, as well as its gradient at all latitudes, is important for describing GCR propagation. A more detailed description of HMF inversion than in Figure 5 *c* is given in two bottom panels of Figure 6 using SC 24 as an example. While the inversion of HMF polarity and its gradient (at the inner heliospheric boundary and the longitude-averaged HMF polarity, its polar angle derivative $(\partial F/\partial\theta)$ plays this role) occurs not quite synchronously at different latitudes, the entire HMF inversion process at the inner heliospheric boundary lasts for about one year.

Note that a fairly similar HMF inversion model has been proposed in [Kopp et al., 2021]. The authors also use the maps of radial magnetic field polarity and shape of current sheets $B_r^{in}=0$ at the inner heliospheric boundary, rather than calculated shapes of current sheets, and try to reduce the polarity distribution to expressions (2), (3) corresponding to the TCS model, but with an arbitrary, not equal only to +1 or –1, overall polarity A in (2). As for the large scales of the heliosphere, Kopp et al. [2021] discuss both the layered model of the heliosphere and the time averaging on its inner boundary.

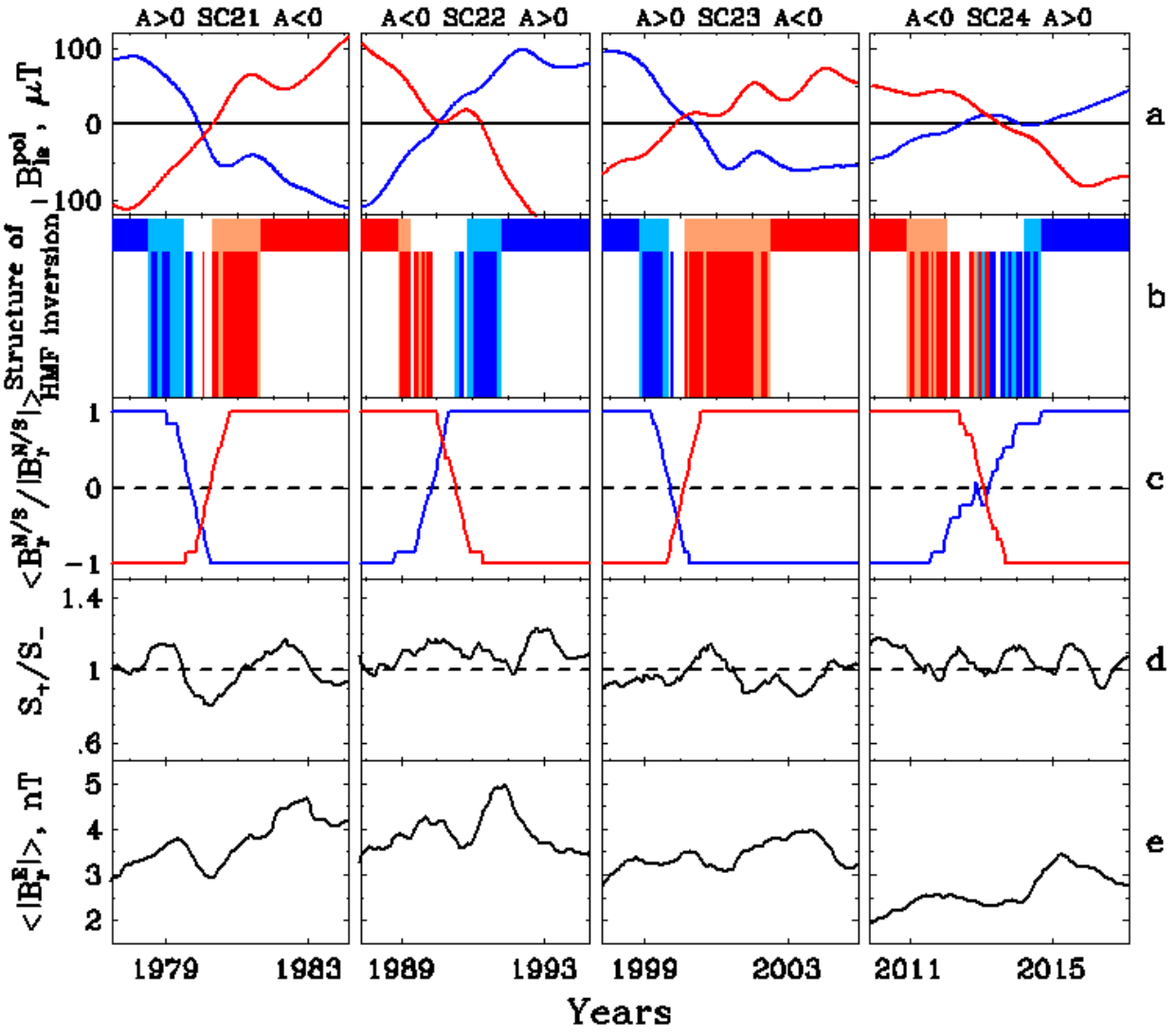

Figure 5. Inversion of magnetic fields on the Sun and at the inner heliospheric boundary and smoothed heliospheric characteristics for maxima of SC 21–24: *a*, *b* are the same as in Figure 2; *c*–*e* are polarities smoothed with a period of 13 solar rotations at the inner heliospheric boundary of HMF of the northern (blue line) and southern (red line) poles (*c*); the ratio of areas with positive and negative HMF polarities (*d*); *e* is the longitude-averaged absolute value of the HMF radial component in Earth's orbit [http://omniweb.gsfc.nasa.gov/]

5. SIMULATION OF GCR INTENSITY IN THE MODEL OF HMF INTERNAL INVERSION

Long-term GCR intensity variations are generally simulated by solving a stationary 3D equation for the distribution function, $\mathcal{U}(\mathbf{r}, p) = J(\mathbf{r}, T)/p^2$, [Parker, 1958, 1965; Krymskiy, 1964; Jokipii et al., 1977]:

$$\nabla\cdot(\mathcal{K}_s\nabla\mathcal{U}) - (\mathbf{V}+\mathbf{V}_d)\cdot\nabla\mathcal{U} + \frac{\nabla\cdot\mathbf{V}}{3}\frac{\partial\mathcal{U}}{\partial\ln p} = 0, \quad (4)$$

where p, T are the momentum and kinetic energy of particles; $\mathcal{K}_s$ is the diffusion tensor; $\mathbf{V}$ and $\mathbf{V}_d$ are SW and particle drift velocities in inhomogeneous HMF.

In this paper, we solve the equation to describe the behavior of the longitude-averaged GCR intensity, $J(r, \theta, T) = \langle J(\mathbf{r}, T)\rangle_\varphi$, which is derived by averaging Equation (2) over longitude:

$$\nabla\cdot(\mathbf{K}\cdot\nabla U) - (\mathbf{V}+\mathbf{V}_d)\cdot\nabla U + \frac{\nabla\cdot\mathbf{V}}{3}\frac{\partial U}{\partial\ln p} = 0, \quad (5)$$

where coefficients of 2D equation (5) are equal to respective longitude-averaged coefficients of 3D equation (4). In this case, on the left-hand side of (5), the poorly known term of the source Q is omitted which depends on longitude variations in $\mathcal{U}(\mathbf{r}, p)$ and coefficients of (2) [Kalinin, Krainev, 2014; Kalinin et al., 2021]. The boundary value problem for $U(r, \theta, p)$ in the spherical heliocentric coordinate system (r, θ, φ) is derived by adding the boundary and initial conditions for U to (5):

$$\partial U/\partial r\big|_{r=r_{in}} = 0,$$
$$\partial U/\partial\theta\big|_{\theta=0,\pi} = 0, \quad (6a)$$
$$U\big|_{r=r_{out}} = U_{nm}(p), \quad (6b)$$
$$U\big|_{p=p_{max}} = U_{nm}(p_{max}), \quad (6c)$$

where r_{in}, r_{out}, U_{nm} are the inner and outer dimensions of the modulation domain and the unmodulated GCR distribution function respectively.

In the calculations, the simplest spherical model of the heliosphere (r_{in}=0.1 AU, r_{out}=122 AU) and a constant radial SW velocity V_{sw}=450 km/s were employed, which is justified in the first approximation for high solar activity [Smith, 2011].

The unmodulated proton spectrum, as well as the spatial and rigidity dependence of the diffusion coefficients in the directions parallel and perpendicular to the regular HMF are also often applied (e.g., [Vos, Potgieter, 2015]):

$$K_{\parallel} = \left(K_{\parallel}\right)_0 \beta \left(\frac{B_0}{B}\right) R^{c1} \left(\frac{R^{c3}+R_k^{c3}}{1+R_k^{c3}}\right)^{\frac{c2_{\parallel}-c1}{c3}}, \qquad (7)$$

$$K_{\perp} = 0.02\, K_{\parallel},$$

with $\left(K_{\parallel}\right)_0 = 0.29 \cdot 10^{22}$ cm^2/s, and B_0=1 nT, R_k=3, c1=0.88, c2=2.1, c3=2.4.

When calculating the GCR behavior during HMF inversion in describing the magnetic field by expression (1), the velocity of magnetic drift of particles (see [Burger, et al., 1985]) is as follows:

$$\mathbf{V}_d = \frac{pv}{3q}\left[\nabla \times \frac{\mathbf{B}}{B^2}\right] = \frac{pv}{3q} F \left[\nabla \times \frac{\mathbf{B}^m}{B^2}\right] + \\ + \frac{pv}{3q}\left[\nabla F \times \frac{\mathbf{B}^m}{B^2}\right], \qquad (8)$$

where p, v, q are particle momentum, velocity, and charge. The first and second terms on the right-hand side of the expression represent particle magnetic drift velocities, regular and along HCS, respectively.

In this paper, we use the solution of the above boundary value problem only to verify one of the main conclusions drawn by Krainev et al. [2023b] from observations of GCR intensity during HMF inversion, namely that during this period for about two years GCR particles of different charges behave almost identically,

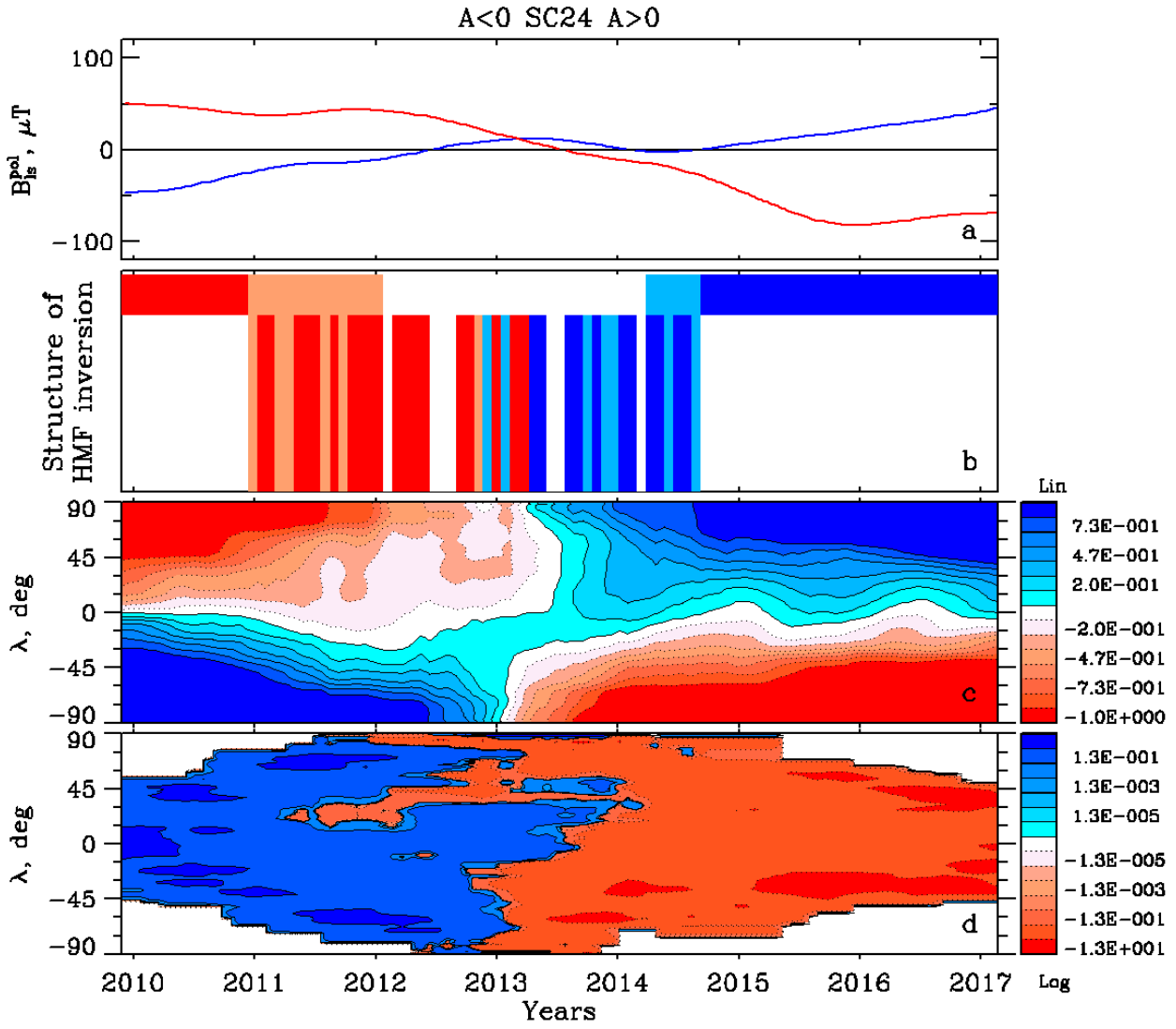

Figure 6. Structure and behavior of HMF inversion at all latitudes in SC 24: *a*, *b* are the same as in the corresponding panels of Figures 2 and 5; *c*, *d* are the longitude-averaged HMF polarity F and its polar angle derivative $\partial F/\partial\theta$ smoothed with 1-year period (see explanation in the text), respectively, at all latitudes. The correspondence of the color with value and sign of the characteristics is shown in the panels on the right

although outside this period the intensity depends on both particle charge q and HMF polarity A. This conclusion was made for the HMF inversion in SC 24 when detailed data on GCR intensity of various types was first obtained from the AMS-02 experiment [Aguilar et al., 2018, 2021], and it is not yet possible to reliably verify it for other periods of HMF inversion.

The only mechanism in boundary value problem of GCR modulation (5), (6) depending on the sign of q is the magnetic drift with velocity (8) determined by the product of q and A. We, therefore, consider the criterion for evaluating the HMF inversion model for a certain SC to be insensitivity of the GCR intensity, calculated by this model, to a change in the sign of particle charge and HMF polarity for about a year or two. Note that the conclusion about the need to completely turn off the particle drift during the HMF inversion in SC 24 for the theoretical description of a set of GCR intensity observations has also been drawn in many works, for example [Aslam et al., 2023].

We will test the HMF inversion model described in Section 4 for SC 24, using the criterion formulated above. In three top panels of Figure7, *a–c*, vertical lines denote the time of three rotations separated by two Carrington rotations. The bottom panel of Figure 7, *d* for these three moments shows the particle spectra calculated when solving (5), (6). For each moment, three spectra obtained when using the drift velocity multiplied by a coefficient equal to 1, –1, 0 have been calculated. These three spectra are indicated respectively by solid blue and red lines and a dashed black line. It is known that during the inversion period of SC 24, HMF polarity varies from A<0 to A>0, and the relative position of the spectra at low energies in the order of increasing intensity corresponds to $qA<0$, $qA=0$, $qA<0$. Thus, a significant discrepancy and a change in the order of the blue and red lines during the transition from the first to the third moment implies that between these moments (just before the second moment) there was a rapid change in the HMF polarity effective for GCRs. This means that the period when the GCR intensity is insensitive to HMF polarity is no more than 3–5 solar rotations, which, when modeling GCRs, contradicts the conclusion that this period is about two years. The HMF inversion model proposed in [Kopp et al., 2021], presumably, has this disadvantage too because it also takes into account only the processes in the layer between the photosphere and the heliosphere.

6. DISCUSSION AND CONCLUSIONS

The description of the stages of layer-by-layer HMF formation in Section 1 generally reflects the great efforts being made in this regard. Nevertheless, the most important and unresolved problem remains the description of SW acceleration, which is due to the lack of a satisfactory theory of this acceleration and, eventually,

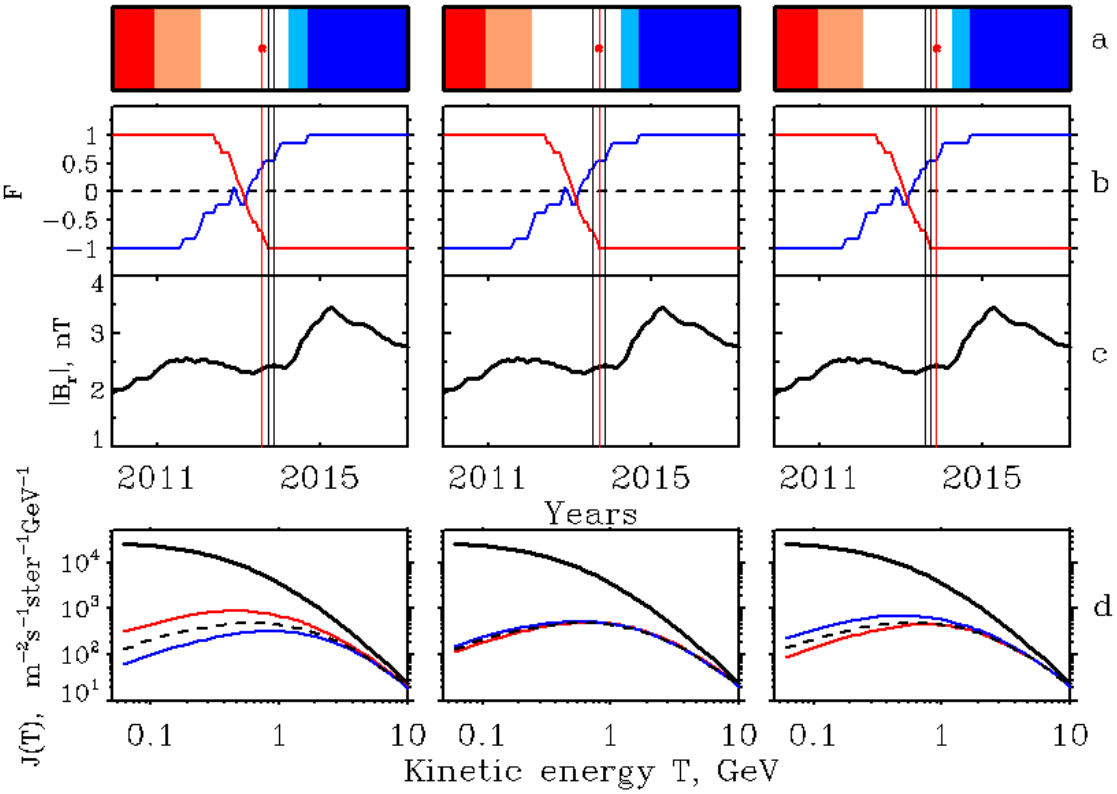

Figure 7. Calculated GCR proton spectra for three Carrington rotations (three vertical columns of the panels) of the inversion period in SC 24, for which the magnetic cycle phases, the smoothed averaged HMF polarity at the poles, and the smoothed HMF radial component modulus are shown respectively in three top horizontal layers of panels *a–c*. Vertical lines in these three panels indicate three moments, with the line for the current rotation denoted in red and marked with an asterisk in the top panel. Three bottom panels *d* illustrate GCR proton spectra for three magnetic drift velocities described in the text

solar corona heating. The SW velocity distribution at the inner heliospheric boundary is, therefore, formed by semi-empirical velocity relationships with the geometry of magnetic field lines and is not very reliable. It is, however, this velocity distribution that determines HMF in the heliosphere itself.

When formulating our qualitative concepts of HMF inversion in Section 2, we have used only WSO data and models, although there are other observatories scanning solar magnetic fields whose data is employed to restore SW velocity fields and HMF at the inner heliospheric boundary. First of all, this is due to the fact that data and calculation results from WSO models have been available since 1976, and data from other observatories and results of simulation of the SW velocity fields and HMF at the inner heliospheric boundary have become available only recently. Nonetheless, when the WSO data is unreliable (for example, at the end of 2022), we use and will continue to use other data [http://gong.nso.edu; http://solarstation.ru/sun-service].

When compare SC 24 and 25 with other cycles and discuss the smoothness (and linearity) of transitions from the Gleisberg Minimum to the Modern Maximum and then return to the Modern Minimum similar to the Gleisberg one (see Section 3), we have relied only on the linearity of four maximum values in the first transition and three in the second. Nevertheless, this very linearity with high correlation coefficients may indicate that these three extremums (Gleisberg Minimum — Modern Maximum — Modern Minimum) are somehow interrelated and differ from other global extremums such as Dalton or Maunder minima that appear suddenly.

Note that when constructing quantitative models of HMF inversion in Section 4, as well as when simulating the GCR intensity in Section 5, longitude averaging during the transition from 3D to 2D models can easily lead to non-physical pattern of the models (for example, to violation of nondivergent HMF) and, possibly, to uncontrolled errors in calculations. It is, therefore, necessary, if possible, to formulate and solve 3D problems with subsequent averaging of the results over longitude, even when a longitude-averaged characteristic is of interest.

In addition, it should be noted that the heliosphere size accounting scheme described in Section 4 assumes that the characteristics observed deep in the heliosphere are transferred at a constant velocity and their distribution does not vary with distance. This second assumption is employed in the HMF inversion model discussed in this paper, as well as in most papers on theoretical description of GCR modulation. Krainev et al. [2023a] have suggested that even during low activity with a stable but nonuniform distribution of SW velocity at the base of the heliosphere the interaction between different-speed SW fluxes can significantly distort the distribution of both SW and GCRs with distance away from the Sun. Moreover, such a distortion of the distribution of heliospheric characteristics with distance should be expected for periods of high sunspot activity and HMF inversion when the SW velocity and HMF distributions at the base of the heliosphere are highly nonuniform and change rapidly. We, therefore, consider the HMF inversion model presented in this paper as the first approximation to a model that adequately describes the situation. On the other hand, it is the processes in the basement of the heliosphere, where magnetic fields are an active agent forming SW and HMF distributions at the inner heliospheric boundary, that lead to HMF inversion. Processes in the heliosphere itself, where the distributions of all characteristics are formed primarily by the solar wind, disturb the HMF inversion already created at the inner boundary.

The main conclusions:

- We have formulated a qualitative model of HMF inversion for solar cycles 21–24, which allows us to present time boundaries, phases, and structure of this phenomenon with respect to HMF polarity distribution.
- In SC 24–25, both the toroidal and poloidal solar activity branches are lower than those during previous cycles belonging to the Modern Maximum, and their level is close to average cycles of the Gleisberg Minimum. The transition from the Gleisberg Minimum to the Modern Maximum and the return again to a level similar to the Gleisberg Minimum occurs linearly in time.
- For each of SC 21–24, we have formulated the so-called internal model of HMF inversion, in which only the solar magnetic field in the photosphere and in the solar corona is an active agent, although finite scales of the heliosphere are taken into account in this case.
- Consideration of GCR intensity modulation in the heliosphere with the aid of the internal model of HMF inversion for SC 24 leads to the conclusion that the HMF inversion is very rapid, i.e. the period when the GCR intensity is insensitive to HMF polarity lasts only 3–5 solar rotations. This sharply contradicts the results of GCR intensity simulation according to which this period is approximately two years.
- To develop a full-fledged HMF inversion model, it is necessary to take into account the disturbance generated at the inner boundary of HMF distribution in the heliosphere per se due to the interaction between inhomogeneous and nonstationary SW streams.

We are grateful to all the teams of researchers who present their results on the Internet. We also thank the reviewers whose comments significantly improved the paper.

REFERENCES

Adriani O., Barbarino G.C., Bazilevskaya G.A., Bellotti R., Boezio M., Bogomolov E.A., et al. (PAMELA collaboration). Time dependence of the proton flux measured by PAMELA during the 2006 July–2009 December solar minimum. *Astrophys. J.* 2013, vol. 765, p. 91. DOI: 10.1088/0004-637X/765/2/91.

Adriani O., Barbarino G.C., Bazilevskaya G.A., Bellott R., Boezio M., Bogomolov E.A., et al. (PAMELA collaboration). Unexpected cyclic behavior in cosmic-**r**ay protons observed by PAMELA at 1 au. *Astrophys. J. Lett*. 2018, vol. 852, p.

L28. DOI: 10.3847/2041-8213/aaa403.

Aguilar M., et al. (AMS Collaboration). Observation of complex time structures in the cosmic-ray electron and positron fluxes with the Alpha Magnetic Spectrometer on the International Space Station. *Phys. Rev. Lett*. 2018. vol. 121. 051102. DOI: 10.1103/PhysRevLett.121.051102.

Aguilar M., et al. (AMS Collaboration). Periodicities in the daily proton fluxes from 2011 to 2019 measured by the Alpha Magnetic Spectrometer on the International Space Station from 1 to 100 GV. *Phys. Rev. Lett.*. 2021, vol. 127, 271102. DOI: 10.1103/PhysRevLett.127.271102.

Altschuler M.D., Newkirk G. Jr. Magnetic fields and the structure of the solar corona. I. Methods of calculating coronal fields. *Solar Phys*. 1969, vol. 9, pp. 131–149. DOI: 10.1007/BF00145734.

Aslam O.P.M., Luo Xi, Potgieter M.S., Ngobeni M.D. Song Xiaojian. Unfolding drift effects for cosmic rays over the period of the Sun's magnetic field reversal. *Astrophys. J*. 2023, vol. 947, iss. 2, id. 72, 17 p. DOI: 10.3847/1538-4357/acc24a.

Boschini M.J., Della Torre S., Gervasi M., Della Torre S., Gervasi M., La Vacca G., Rancoita P.G. Propagation of cosmic rays in heliosphere: The HelMod model. *Adv. Space Res*. 2018, vol. 62, iss. 10, pp. 2859–2879. DOI: 10.1016/j.asr.2017.04.017.

Burger R.A., Moraal H., Webb G.M. Drift theory of charged particles in electric and magnetic fields. *Astrophys. Space Sci*. 1985, vol. 116, iss. 107.

Charbonneau P. Dynamo models of the solar cycle. *Living Reviews Solar Physics*. 2010, vol. 7, article number 3, p. 3.

Gnevyshev M.N. On the 11-year cycle of solar activity. *Solar Phys*. 1967, vol. 1, pp. 107–120, DOI: 10.1007/BF00150306.

Guo X., Florinski V. Corotating interaction regions and the 27 day variation of galactic cosmic rays intensity at 1 AU during the cycle 23/24 solar minimum. *J. Geophys. Res.: Space Phys*. 2014, vol. 119, iss. 14, pp. 2411–2429. DOI: 10.1002/2013 JA019546.

Guo X., Florinski V. Galactic cosmic-ray intensity modulation by corotating interaction region stream interfaces at 1 AU. *Astrophys. J*. 2016, vol. 826:65, no. 1. DOI: 10.3847/0004-637X/826/1/65.

Jokipii J.R., Levy E.H., Hubbard W.B. Effects of particle drift on cosmic-ray transport. I. General properties, application to solar modulation. *Astrophys. J*. 1977, vol. 213, pp. 861–868. DOI: 10.1086/155218.

Jokipii J.R., Thomas B. Effect of drift on the transport of cosmic rays. IV. Modulation by a wavy interplanetary current sheet. *Astrophys. J*. 1981, vol. 243, pp. 1115–1122. DOI: 10.1086/ 158675.

Kalinin M.S., Krainev M.B. Two-dimensional transport equation for galactic cosmic rays as a consequence of a reduction of the three-dimensional equation. *Geomagnetism and Aeronomy*. 2014, vol. 54, no. 4, pp. 423–429. DOI: 10.1134/S0016793214040045.

Kalinin M.S., Krainev M.B., Gvozdevsky B.B., Aslam O.P.M., Ngobeni M.D., Potgieter M.S. On the transition from 3D to 2D transport equations for a study of long-term cosmic-ray intensity variations in the heliosphere *PoS ICRC2021*. 2021. 1323. DOI: 10.22323/1.395.1323.

Kopp A., Raath J.L., Fichtner H., Kühl P., Kopp A., Heber B., Kissmann R. Cosmic-ray transport in heliospheric magnetic structures. III. Implications of solar magnetograms for the drifts of cosmic rays. *Astrophys. J*. 2021, vol. 922:124. DOI: 10.3847/1538-4357/ac23e0.

Krainev M.B. Manifestations of two branches of solar activity in the heliosphere and GCR intensity. *Solar-Terr. Phys*. 2019, vol. 5, iss. 4, pp. 10–20. DOI: 10.12737/stp-54201902.

Krainev M.B., Kalinin M.S., The models of the infinitely thin global heliospheric current sheet. Proc. 12th International Solar Wind Conference. Saint-Malo, AIP Conference Proc. 2010, vol. 1216, pp. 371–374.

Krainev M.B., Kalinin M.S. On the GCR intensity and the inversion of the heliospheric magnetic field during the periods of the high solar activity. *Proc. 33rd International Cosmic Ray Conference*. 2014, icrc2013-0317/1-4, ArXiv:1411.7532 [astro-ph.SR].

Krainev M., Bazilevskaya G., Kalinin M., Svirzhevskaya A., Svirzhevsky N. GCR intensity during the sunspot maximum phase and the inversion of the heliospheric magnetic field. *Proc. Science*. 2015, PoS (ICRC2015) 081/1-8.

Krainev M., Kalinin M., Aslam O.P.M., Ngobeni D., Potgieter M. On the dependence of maximum GCR intensity on heliospheric factors for the last five sunspot minima *Adv. Space Res.* 2021, vol. 68, iss. 7, pp. 2953–2962. DOI: 10.1016/j.asr. 2021.05.021.

Krainev M.B., Kalinin M.S., Bazilevskaya G.A., Svirzhevskaya A.K., Svirzhevsky N.S., Xi Luo, Aslam O.P.M., Fang Shen, Ngobeni M.D., Potgieter M.S. Manifestation of solar wind corotating interaction regions in GCR intensity variations. *Solar-Terr. Phys*. 2023a, vol. 9, iss. 1, pp. 9–20. DOI: 10.12737/stp-91202302.

Krainev M.B., Bazilevskaya G.A., Kalinin M.S., Mikhailov V.V., Svirzhevskaya A.K., Svirzhevsky N.S. Fifty years of studying the GCR intensity during inversion of heliospheric magnetic fields I. Observations. *Solar-Terr. Phys*. 2023b, vol. 9, iss. 4, pp. 3–16. DOI: 10.12737/stp-94202301.

Krymskiy G.F. Diffusion mechanism of diurnal cosmic-ray variation. *Geomagnetizm i Aeronomiya* [Geomagnetism and Aeronomy]. 1964, vol. 4, pp. 763–769.

Luo X., Feng X., Shen F., Zhang M., Potgieter M. A numerical study of the effects of corotating interaction regions on cosmic-ray transport. *Astrophys. J*. 2020, vol. 899:90, no. 2. DOI: 10.3847/1538-4357/aba7b5.

Odstrcil D. Modeling 3-D solar wind structure. *Adv. Space Res*. 2003, vol. 32, iss. 4, pp. 497–506. DOI: 10.1016/S0273-1177(03)00332-6.

Parker E.N. Cosmic ray modulation by solar wind. *Phys. Rev*. 1958, vol. 110, p. 1445. DOI: 10.1103/PhysRev.110.1445.

Parker E.N. The passage of energetic charged particles through interplanetary space. *Planetary and Space Sciences*. 1965, vol. 13, pp. 9–49. DOI: 10.1016/0032-0633(65)90131-5.

Potgieter M.S. Solar modulation of cosmic rays. *Living Revs. Solar Phys*. 2013, vol. 10, p. 3. DOI: 10.12942/lrsp-2013-3.

Rosenberg R.L., Coleman P. Heliographic latitude dependence of the dominant polarity of the interplanetary magnetic field. *J. Geophys. Res*. 1969, vol. 74, iss. 24, p. 5611. DOI: 10.1029/JA074i024p05611.

Schatten K.H. Current sheet magnetic model for the solar corona. *Cosmic Electrodymanics*. 1971, vol. 2, p. 232.

Schatten K.H., Wilcox J.M., Ness F.N. A model of interplanetary and coronal magnetic fields. *Solar Phys*. 1969, vol. 6, pp. 442–455.

Schove D.J. Sunspot cycles, Hutchinson Ross. Publ., Stroudburg, PA, USA. 1983.

Sheeley N.R., Jr. Polar faculae during the interval 1906–1975. *J. Geophys. Res*. 1976, vol. 81, p. 3462. DOI: 10.1029/JA081i019p03462.

Sheeley N.R., Jr. A century of polar faculae variations. *Astrophys. J*. 2008, vol. 680, pp. 1553–1559. DOI: 10.1086/588251.

Shulz M. Interplanetary sector structure and the heliomagnetic equator. *Astrophys. Space Sci*. 1973, vol. 24, p. 371. DOI: 10.1007/BF02637162.

Smith E.J. Solar cycle evolution of the heliospheric mag-

netic field: The Ulysses legacy. *J. Atmos. Solar-Terr. Phys*. 2011, vol. 73, iss. 2-3, pp. 277–289. DOI: 10.1016/j.jastp.2010.03.019.

Storini M., Bazilevskaya G.A., Fluckiger E.O., Krainev M.B., Makhmutov V.S., Sladkova A.I. The Gnevyshev gap: A review for space weather. *Adv. Space Res*. 2003, vol. 31, no. 4, pp. 895–900. DOI: 10.1016/S0273-1177(02)00789-5.

Stozhkov Yu.I., Okhlopkov V., Makhmutov V., Logachev V. Solar activity, cosmic rays, and global climate changes. *Proc. 33rd International Cosmic Ray Conference*. 2013. P. 1607.

Tóth G., van der Holst B., Sokolov I.V., De Zeeuw D.L., Gombosi T.I., Fang F., Manchester W.B. Adaptive numerical algorithms in space weather modeling. *J. Computational Physics*. 2012, vol. 231, iss. 3, p. 870903. DOI: 10.1016/j.jcp.2011.02.006.

Vos E.E., Potgieter M.S. New modeling of galactic proton modulation during the minimum of solar cycle 23/24. *Astrophys. J*. 2015, 815:119. DOI: 10.1088/0004-637X/815/2/119.

Wiengarten T., Kleimann J., Fichtner H., Kühl P., Kopp A., Heber B., Kissmann R. Cosmic ray transport in heliospheric magnetic structures. I. Modeling background solar wind using the CRONOS magnetohydrodynamic code. *Astrophys. J*. 2014, vol. 788:80. DOI: 10.1088/0004-637X/788/1/80.

Zhao X., Hoeksema J.T. A coronal magnetic field model with horizontal volume and sheet currents. *Solar Phys*. 1994, vol. 151, iss. 1, pp. 91–105. DOI: 10.1007/BF00654084.

URL: http://wso.stanford.edu (accessed July 7, 2024).

URL: http://gong.nso.edu/ (accessed July 7, 2024).

URL: http://solarstation.ru/sun-service (accessed July 7, 2024).

URL: https://www.gaoran.ru/database/esai (accessed July 7, 2024).

URL: https://solarscience.msfc.nasa.gov (accessed July 7, 2024).

URL: ftp://ftp.swpc.noaa.gov/pub/forecasts/SRS/ (accessed July 7, 2024).

This paper is based on material presented at the 19th Annual Conference on Plasma Physics in the Solar System, February 5–9, 2024, IKI RAS, Moscow.

Original Russian version: Krainev M.B., Kalinin M.S., published in Solnechno-zemnaya fizika. 2024. Vol. 10. No. 3. P. 40–52. DOI: 10.12737/szf-103202405. © 2024 INFRA-M Academic Publishing House (Nauchno-Izdatelskii Tsentr INFRA-M)

How to cite this article

Krainev M.B., Kalinin M.S. Fifty years of studying the GCR intensity during inversion of the heliospheric magnetic fields. II. HMF inversion on the inner heliospheric boundary. *Solar-Terrestrial Physics*. 2024. Vol. 10. Iss. 3. P. 37–49. DOI: 10.12737/stp-103202405.